JOURNAL OF Materials CHEMISTRY

Towards elucidating microscopic structural changes in Li-ion conductors $Li_{1+y}Ti_{2-y}Al_y[PO_4]_3$ and $Li_{1+y}Ti_{2-y}Al_y[PO_4]_{3-x}[MO_4]_x$ (M = V and Nb): X-ray and ^{27}Al and ^{31}P NMR studies

Shan Wong,[a] Peter J. Newman,[b] A. S. Best,[b] K. M. Nairn,[a] D. R. MacFarlane[b] and Maria Forsyth*[a]

[a] *Department of Materials Engineering and* [b] *Department of Chemistry, Monash University, Wellington Road, Clayton, Victoria 3168, Australia. E-mail: maria.forsyth@eng.monash.edu.au*

Received 14th April 1998, Accepted 17th July 1998

A combination of X-ray powder diffraction (XRD) and nuclear magnetic resonance (NMR) studies has demonstrated that attempted substitutions of Al, V and Nb into the framework of $LiTi_2(PO_4)_3$ yield several impurity phases in addition to direct substitutions of Al into Ti and V, Nb into P sites. Direct substitutions were confirmed by changes in the unit cell dimensions as indicated by the peak shifts observed in the X-ray diffractographs and by analyses of the ^{27}Al and ^{31}P magic angle spinning (MAS) spectra. A major impurity phase was identified as $AlPO_4$ (found in at least two polymorphs) and the amount present increases with increasing Al additions. The formation of $AlPO_4$ appeared to be enhanced by further V but suppressed by Nb substitution. These results suggest that the presence of $AlPO_4$, together with the non-stoichiometric modified LTP, may be the cause for the observed densification of this material upon sintering and the increased ionic conductivity.

Introduction

Lithium ion conducting $LiTi_2[PO_4]_3$ (LTP) is a microporous ceramic based on a NASICON framework structure of $[PO_4]^{3-}$ tetrahedra and $[TiO_6]^{8-}$ octahedra in corner sharing arrangements.[1,2] A representation of the NASICON structure is shown in Fig. 1. Mobile Li^+ cations occupy interstitial positions to achieve electroneutrality. Hence, these materials are potentially useful in lithium battery applications. Li ion mobility and thereby the Li ionic conductivity are influenced by sizes of the polyhedral cations and ionicity of the Li···O bond.

By substitution of trivalent cations for Ti^{4+} cations in the octahedral sites of $LiTi_2[PO_4]_3$ (LTP), Aono *et al.* reported much improved Li ionic conductivity in the modified ceramics.[3,4] Further pentavalent cation substitution into the tetrahedral phosphorus sites (*e.g.* using V, Nb, Ta) can also be carried out. Among the modified LTP ceramics, Al substituted LTP at the nominal composition $Li_{1.3}Al_{0.3}Ti_{1.7}[PO_4]_3$ (LATP) was reported by Aono *et al.* to have the optimum Li ionic conductivity (bulk 3×10^{-3}, grain boundary 9×10^{-4}, and total 7×10^{-4} S cm^{-1}). Similar bulk conductivities for LATP have been reproduced in our laboratory ($\approx2\times10^{-3}$ S cm^{-1}), although the grain boundary conductivities were found to be highly dependent on processing conditions.[5] The improved conductivity was attributed by Aono *et al.* to the densification of the sintered pellet and to a decrease in activation energy for the grain boundary ion transport. The activation energy for the bulk conductivity remained unaffected by the Al^{3+} substitution. The question remains as to the origin for the higher degree of densification in the modified material. The exact nature of site substitution, and its effect on the framework structure, has also yet to be elucidated.

In an earlier solid state nuclear magnetic resonance (NMR) study, tetrahedral and octahedral Al signals were observed in LATP, when only an octahedral signal for the Al in the octahedral (Ti) sites was expected.[6] Here, a systematic concentration-dependent study on the modified ceramics, namely $Li_{1+y}Al_yTi_{2-y}(PO_4)_3$ (LATP) and $Li_{1+y}Al_yTi_{2-y}(PO_4)_{3-x}(MO_4)_x$ (M = V^{5+}, Nb^{5+}) (V-LATP and Nb-LATP), is presented. The aim is to investigate the origin of the two aluminium signals, to clarify the solid state reactions, and to understand the exact nature of site substitution, as part of a continuing effort in determining the effect of framework modification on Li ion mobility. X-Ray powder diffraction and high resolution solid state NMR spectroscopy are used.

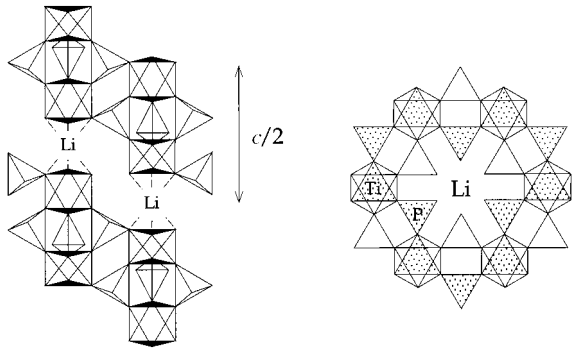

Fig. 1 A representation of the NASICON structure (adopted from ref. 3), showing the unit cell stacking along the *c*-axis (left) and its projection onto the basal plane (right). Lithium cations occupy interstitial positions surrounded by six phosphate tetrahedra and sandwiched by two titanium octahedra.

Experimental

Appropriate ratios of $(NH_4)_2HPO_4$, TiO_2, Li_2CO_3, Al_2O_3 for LATP (and V_2O_5 or Nb_2O_5 for V/Nb-LATP) were mixed and the mixture was placed in a graphite crucible and heated to and held at 300 °C until ammonia, carbon dioxide, and water evolution ceased. The coarse solid was ground and passed through a 250 micrometer sieve before being heated at 400 °C in a platinum crucible for 1 h, followed by 950 °C for 2 h. The reaction was carried out under a continuous flow of Ar(25%)–O_2 to prevent reduction of the transition metal cations. The reaction product was ball milled in ethanol, and the resultant particle size was estimated to be <2 μm by SEM (JEOL JSM 840-A). X-Ray powder diffractographs (Rigaku Geiger-flex) were acquired to confirm reaction products. In addition to peaks corresponding to LTP, low intensity peaks were observed which suggest the presence of residual amounts

of impurities (estimated to be $<5\%$). The significance of these impurity phases will be discussed.

NMR experiments were carried out in a 7.05 T superconducting magnet (Oxford Instruments) equipped with a Bruker CXP 300 spectrometer operated by a Tecmag interface (Minimacspect). Room temperature magic angle spinning (MAS) spectra were acquired using a MAS probe (Bruker HP-WB, 4 mm zirconia rotor and Kel-F endcap) at the maximum spinning speed of 14 kHz. Typical radio frequency pulses of 2 μs for ^{31}P and 0.6 μs for ^{27}Al (1/3 of 'π/2' pulse) were used. All ^{27}Al spectra were accumulated over 64 transients with a 40 s recycle delay. ^{31}P spectra were averaged over four scans with a 40 s delay between scans. ^{27}Al and ^{31}P chemical shifts were externally referenced to $[Al(H_2O)_6]^{3+}$ and 85% H_3PO_4, respectively.

Results and discussion

Results

X-Ray powder diffraction. Fig. 2 shows X-ray powder diffraction patterns taken for LATP samples of varying Al concentration. Major reflections were assigned according to the previously reported powder diffraction for LTP.[7] The main reaction product was confirmed to be rhombohedral of space group $R\bar{3}c$ (analogous to NASICON). The diffraction patterns for LTP, LATP, V-LATP, and Nb-LATP ($y_{Al}=0.3$, $x_{V,Nb}=0.1$) are shown in Fig. 3 for comparison. Unit cell dimensions derived from structural analyses of the diffraction patterns for $V_{0.1}$-LATP and $Nb_{0.1}$-LATP are given in Table 1, together with results reported for LTP[7] and for LATP.[3]

Cell dimensions for all the modified ceramics are noticeably smaller than LTP, with LATP ($y_{Al}=0.3$) being the smallest. The contraction of the LATP unit cell can be explained to a first order approximation by partial substitution of smaller Al^{3+} for Ti^{4+} ions (0.535 *vs.* 0.605 Å ionic radius). The slight expansion of the unit cell upon V and Nb substitution results from much larger V^{5+} and Nb^{5+} ions occupying the P^{5+} sites (0.355 and 0.48 Å *vs.* 0.17 Å, respectively). An attempt to synthesize single-phased Ta-LATP failed, possibly due to the Ta^{5+} cation being much larger.

Low intensity peaks in the regions 2θ 17–19, 21–24 and 26–29° do not belong to the NASICON structure. In LATP with $y_{Al}<0.3$, two minor phases were identified to be TiO_2 (rutile) and TiP_2O_7 (peaks marked by R and T, respectively). At $y_{Al}=0.3$, new peaks at $2\theta=21.7$ and 35.8° were assigned to $AlPO_4$ of the tridymite phase (peaks marked by A)[8] and

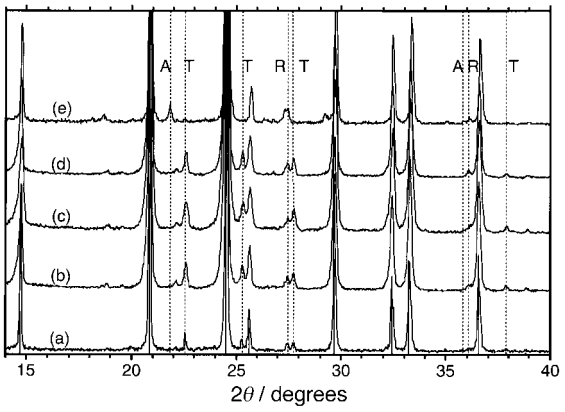

Fig. 2 X-Ray powder diffraction patterns for LATP as a function of increasing Al addition: (a) 0.0, (b) 0.05, (c) 0.1, (d) 0.2 and (e) 0.3. All samples show major reflections corresponding to those observed for LTP (identified by sticks at the base). Small intensities in the regions of $2\theta=17$–19, 21–24 and 26–29° cannot be assigned to LTP and belong to residual phases present (R = TiO_2-rutile, T = TiP_2O_7, and A = $AlPO_4$-tridymite).

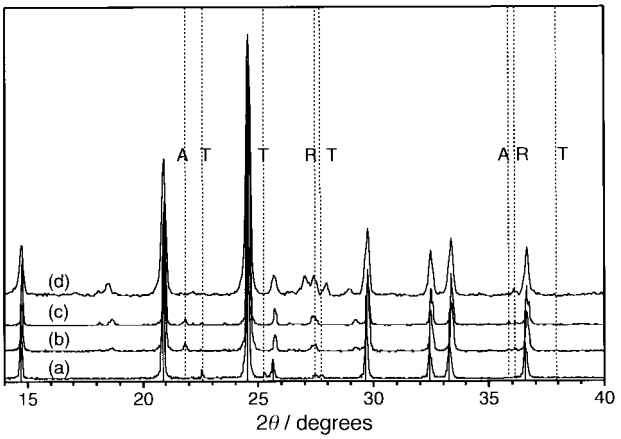

Fig. 3 X-Ray powder diffraction patterns for (a) LTP, (b) LATP ($y_{Al}=0.3$), (c) V-LATP ($y_{Al}=0.3$ and $x_V=0.1$) and (d) Nb-LATP ($y_{Al}=0.3$ and $x_{Nb}=0.1$) plotted for comparison.

Table 1 Unit cell parameters for LTP and LTP-based ceramics

Nominal composition	a/Å	c/Å	β/°	V/Å^3
$LiTi_2(PO_4)_3$[a]	8.5129(8)	20.878(4)	120[b]	1310.3
$Li_{1.3}Al_{0.3}Ti_{41.7}(PO_4)_3$[b]	8.50	20.82	120[b]	1303
$Li_{1.3}Al_{0.3}Ti_{1.7}(PO_4)_{2.9}(VO_4)_{0.1}$	8.5044(6)	20.827(5)	120[b]	1304.5
$Li_{1.3}Al_{0.3}Ti_{1.7}(PO_4)_{2.9}(NbO_4)_{0.1}$	8.5061(6)	20.836(4)	120[b]	1305.6

[a]Ref. 7. [b]Ref. 3.

the intensities of the TiP_2O_7 peaks were much reduced. $AlPO_4$ (tridymite) and rutile, but not TiP_2O_7, were present in the $V_{0.1}$-LATP systems. Intensities of the tridymite peaks increased with increasing Al added to both LATP and V-LATP ceramics (Fig. 2). The sharp reflections of the impurity peaks suggest crystalline phases are present, and the flat baselines indicate the absence of substantial amorphous materials. The diffraction pattern for Nb-LATP [Fig. 3(d)] does not show the prominent presence of $AlPO_4$. The significance of $AlPO_4$ will be discussed in the context of ^{27}Al NMR spectroscopy. Authors of previous X-ray studies of LTP and modified LTP did remark on impurity phases present, but the extra reflections were not documented.[7,9–11]

^{27}Al MAS spectroscopy. In a previous NMR study of LATP ($y_{Al}=0.3$), we observed ^{27}Al resonances at δ −15 and 40 which were assigned to aluminium in octahedral (Al_O) and tetrahedral (Al_T) sites, respectively.[6] Here, ^{27}Al MAS NMR studies were carried out to determine the onset of the Al_T signal. Fig. 4 shows the ^{27}Al spectra as a function of Al concentration in LATP, with a plot of the Al_T/Al_O ratios in the inset. At $y_{Al}<0.2$, only Al_O signals at δ −15 were observed. Since no Al-containing impurities were found in the X-ray diffractographs, we assigned this signal to Al occupying the octahedral Ti sites in LTP, and thus confirm direct Al substitution into the LTP framework. At $y_{Al}=0.2$, the δ 40 Al_T signal appeared, and the Al_T onset is therefore estimated to be between $y=0.1$ and 0.2.

The same concentration-dependent study was carried out for V-LATP and results are shown in Fig. 5. Tetrahedral Al signal was detected at $y_{Al}=0.1$, and the Al_T/Al_O ratios were comparable to those found for LATP. An additional broad resonance around δ 10 was observed in V-LATP ceramics. In contrast to LATP and V-LATP, Nb-substituted LATP (Nb-LATP) showed a much reduced Al_T/Al_O ratio (1:20 at $y_{Al}=0.3$) (Fig. 6).

^{31}P MAS spectroscopy. The effect of Al substitution on the local environment of phosphorus was monitored by ^{31}P NMR

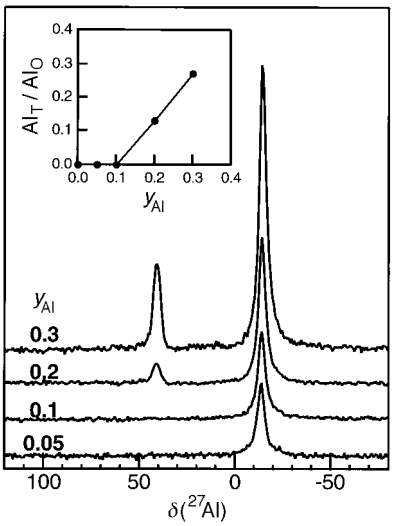

Fig. 4 ^{27}Al MAS spectra of LATP show the concentration dependence of the octahedral (δ −15) and tetrahedral (δ 40) Al signals. The resonance at δ 40 appears at $y_{Al}=0.1$. The ratio of Al_T/Al_O as a function of Al concentration is plotted in the inset, showing a monotonic increase.

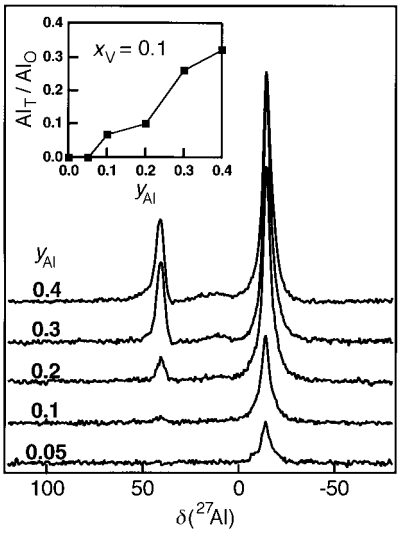

Fig. 5 ^{27}Al MAS spectra for V-LATP show similar concentration dependence observed for LATP. In the presence of vanadium, the onset concentration for the tetrahedral aluminium signal is lowered to 0.1. Similar Al_T/Al_O ratios are found for the concentration range studied.

spectroscopy. Fig. 7 shows the ^{31}P MAS spectra for LTP, and LATP at various Al concentrations. A shift of δ −28 is characteristic of orthophosphates. The LTP spectrum was narrow, while resonances for LATP showed gradual and asymmetric broadening with increasing Al concentration. (Fine spectral shape was observed for the ^{31}P resonance of LTP, the origin of which is not entirely understood).

Changes in the phosphorus environments in V-LATP and Nb-LATP systems were similarly monitored. ^{31}P spectra for V-LATP at a fixed $x_V=0.1$ and varying Al concentration (Fig. 8) showed similar asymmetric broadening observed in the LATP spectra. At $y_{Al}\leqslant 0.1$, however, an additional well resolved ^{31}P resonance at δ −25 was observed, the intensity of which increased with vanadium concentration (Fig. 9). We assign this minor resonance to phosphorus in the vicinity of V-substituted phosphorus sites.[12] A minor ^{31}P resonance was also observed in Nb-LATP at δ −10 (Fig. 10).

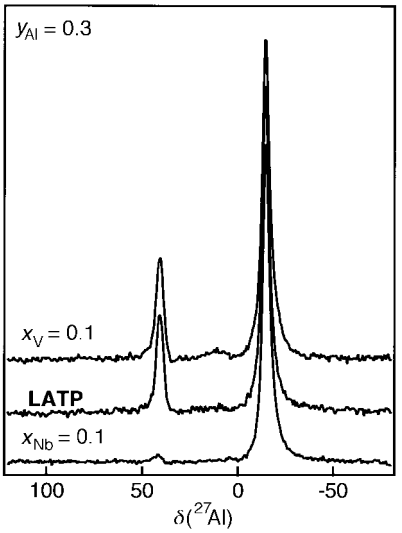

Fig. 6 ^{27}Al MAS spectra for V-LATP, LATP at $y_{Al}=0.3$ show nearly identical Al_T/Al_O ratios of 1/4, while the Nb-LATP spectrum shows that the tetrahedral signal is reduced by Nb substitution.

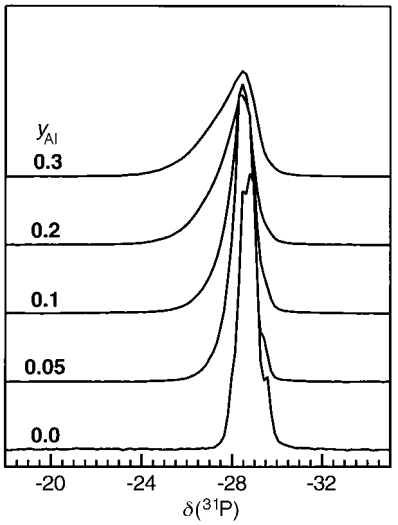

Fig. 7 ^{31}P MAS spectra for LATP show gradual and asymmetric broadening of the ^{31}P resonance with Al concentration. The asymmetric lineshapes are characteristic of a distribution of sites arising from a distribution of M−O−P bond angles.

Discussion

X-Ray powder diffraction. To assign residual reflections in the X-ray diffraction patterns of the Al-modified LTP ceramics requires consideration of the effect of Al substitution. Two hypotheses are considered. First, if Al substitution (at low concentration level) is distributed randomly throughout a crystal (a solid solution), the unit cell dimensions would be modified by the substitution and shifts in the LTP reflections would be observed. Second, if Al incorporation occurs preferentially on the surface of a crystallite (*e.g.* as a grain boundary phase) or in a crystal domain (*e.g.* as trapped impurity), then the structure and symmetry of these Al-containing phases would differ from LTP. In this case, additional reflections would be detected. For the LATP, V-LATP and Nb-LATP ceramics, peak shifts were measured which confirmed changes in the unit cell dimensions as a result of direct polyhedral cation substitutions. The detection of additional peaks indicated that secondary phases are present, some of which have been identified.

The presence of secondary phases requires that the main reaction product (LATP, V-LATP and Nb-LATP) be non-

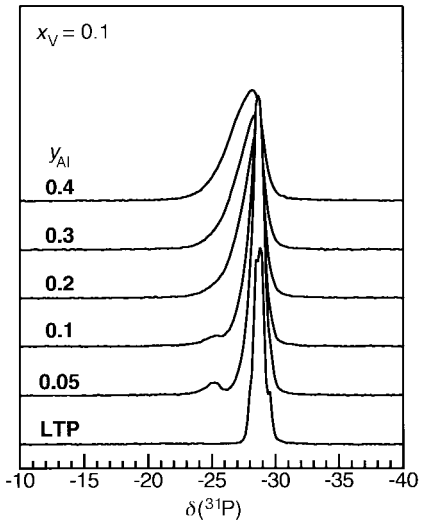

Fig. 8 ^{31}P MAS spectra of $V_{0.1}$-LATP showing similar asymmetric broadening of the phosphorus resonance with increasing substitution. Note that at low Al concentration, a minor resonance at δ −25 is observed and is assigned to phosphorus atoms nearest to V atoms. At high Al concentration, this resonance is obscured by the overlap between the major and minor peaks.

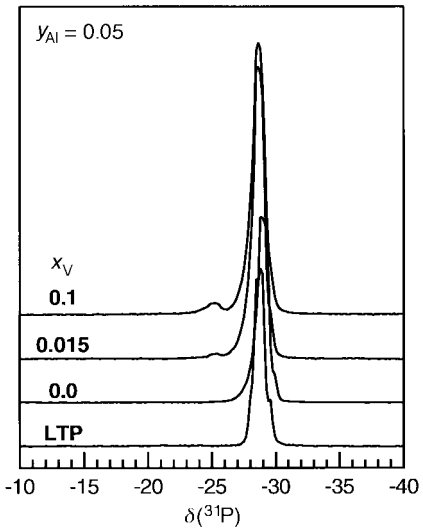

Fig. 9 ^{31}P MAS spectra for V-LATP ($y_{Al}=0.05$) demonstrate that the intensity of the resonance at δ −25 increases with increasing V concentration. This trend is also observed for V-LATP at $y_{Al}=0.1$.

stoichiometric. Both the non-stoichiometry of the modified LTP and the presence of impurity phases may affect pellet densification and the ionic conductivities of these materials. Among the impurity phases found (rutile, TiP_2O_7 and $AlPO_4$), $AlPO_4$ is most interesting as it contains the Al^{3+} cations intended for the Ti sites on the LTP framework (whereas both TiO_2 and TiP_2O_7 are found in the reaction for LTP). Although we are currently unable to pinpoint the location of $AlPO_4$, previous reports have reported its presence in the intergranular regions of titanium phosphate ceramics.[13]

^{27}Al and ^{31}P NMR. The presence of $AlPO_4$ at higher Al concentration (and possibly other yet to be identified Al-containing impurities phases) undoubtedly complicates the interpretation of the tetrahedral ^{27}Al NMR signal at δ 40. The structure of $AlPO_4$ is formed of corner sharing $[PO_4]^{3-}$ and $[AlO_4]^{5-}$ tetrahedra. Three polymorphs exist: berlinite, tridymite and cristobalite (the latter two are isomorphous with

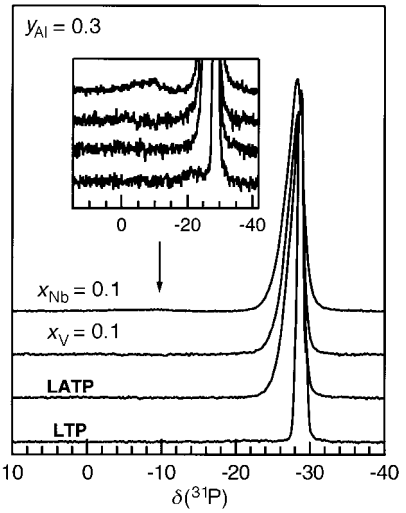

Fig. 10 The ^{31}P spectra for Nb-LATP, V-LATP, LATP (at $y_{Al}=0.3$) and LTP are plotted for comparison. A weak resonance at δ −10 is detected and assigned to those ^{31}P nearing a Nb atom (see the expanded insert).

SiO_2). Transitions between polymorphs occur at,

$$\text{berlinite} \xrightarrow{700\,^\circ C} \text{tridymite} \xrightarrow{1100\,^\circ C} \text{cristobalite}$$

The three polymorphs can be distinguished by X-ray powder diffraction[14] and by ^{27}Al NMR spectroscopy.[15] ^{27}Al resonances for tridymite and cristobalite were found at δ 39 and, owing to much reduced quadrupolar coupling constants, their central transitions were relatively unaffected by second order quadrupolar interactions.[15] On this basis, the δ 40 tetrahedral Al signals observed in LATP and V-LATP at $y_{Al} \geqslant 0.1$ (Fig. 4 and 5) are assigned to the cristobalite and/or tridymite phases of $AlPO_4$. As the tridymite to cristobalite transformation occurs above the reaction temperature of 950 °C, we therefore assign the Al_T signal to tridymite phase of $AlPO_4$. This is in agreement with the assignment made based on the positions of the residual X-ray peaks (2θ at 21.7 and 35.8°), although ^{27}Al NMR spectroscopy proves to be more sensitive than X-ray powder diffraction.

In contrast to tridymite and cristobalite, the berlinite ^{27}Al MAS resonance should be centered at δ 10 and show a stronger second order quadrupolar broadening of its central transition.[15] The broad and low intensity resonance at δ 10 observed in LATP and V-LATP at high Al concentration (Fig. 4 and 5) may possibly be attributable to the Al in berlinite.

The ^{31}P chemical shifts found for the three polymorphs of $AlPO_4$ fall into the shift range of interest (δ *ca.* −28).[15] Hence, we are unable to distinguish the $Al^{31}PO_4$ signal from that of the modified LTP. Owing to low concentrations of these phases, however, their contributions to the total phosphorus signal are considered small. ^{31}P NMR spectroscopy is sensitive to the changes in the P—O—M bond angle, which may affect either or both the magnitude and the orientation of the ^{31}P magnetic shielding (*i.e.* the chemical shift anisotropy tensor). Under magic angle spinning, these changes are reduced to different isotropic chemical shifts. The asymmetric broadening of the ^{31}P resonance in LATP in Fig. 7, therefore, reflects slight changes in the LTP framework upon substitution. This structural change is illustrated by considering a 'chain' of alternating oxide bonds,

$$-(\text{Ti}-\text{O}-\text{P}-\text{O}\cdots\text{Li}\cdots\text{O}-\text{P}-\text{O}-\text{Ti}-\text{O}-\text{P}-\text{O}-)_n$$

in which an Al^{3+} is substituted for the Ti^{4+} as in,

$$-(\text{Ti}-\text{O}-\text{P}-\text{O}\cdots\text{Li}\cdots\text{O}-\text{P}-\text{O}-\text{Al}-\text{O}-\text{P}-\text{O}-)_n$$

Table 2 Electronegativities (EN) and ion radii (Å)

	Li^+	Ti^{4+}	Al^{3+}	P^{5+}	V^{5+}	Nb^{5+}	O^{2-}
EN	0.98	1.54	1.61	2.19	1.63	1.6	3.44
IV: CR[a]	0.73	0.56	0.53	0.31	0.495	0.62	1.24
IR[b]	0.59	0.42	0.39	0.17	0.355	0.48	1.38
VI: CR	0.90	0.745	0.675	0.52	0.68	0.78	1.26
IR	0.861	0.605	0.535	0.38	0.54	0.64	1.40
%[c]	78	59	57	32	56	57	—

[a]Tetrahedral (IV) and octahedral (VI) coordination. CR = covalent radius. [b]IR = ionic radius. [c]% ionic character of oxide bond = $1-\exp(-0.25(\chi_A-\chi_B)^2)$, where $(\chi_A-\chi_B)$ is the difference in electronegativity.

Owing to the size difference between the two cations, the Al—O—P bond angle deviates from that of Ti—O—P, leading to a change in the ^{31}P isotropic shift under the condition of magic angle spinning. Increasing Al incorporation gradually changes the distribution of M—O—P angles to result in an increasingly asymmetric lineshape for phosphorus. In contrast, when a V or Nb atom is placed in a P site (M = V or Nb),

$$-(\text{Ti}-\text{O}-\text{P}-\text{O}\cdots\text{Li}\cdots\text{O}-\text{M}-\text{O}-\text{Ti}-\text{O}-\text{P}-\text{O}-)_n$$

the nearest P is in the second coordination sphere and the P—O—M bond angle change is therefore reduced. Based on this analysis, the asymmetric broadening in the phosphorus spectra reflects mostly structural changes due to Al substitution.

The effects of adding V and Nb to LTP are observed as separate lower intensity ^{31}P resonances in Fig. 9 and 10. The shifts of the minor ^{31}P peaks may reflect changes in the electron density near the substituted site. Table 2 shows that Ti, Al, V, and Nb have similar electronegativity (EN) values[16,17] which are lower than that of P so that substitution of any of these atoms into a P site can alter the local electron density for the nearby phosphorus.

A discussion on structure and mobility. As the modified LTP ceramics are prepared from stoichiometric mixtures of oxides, the presence of impurity phases strongly suggests that the nominal compositions do not represent the actual ceramic compositions. Assuming Li^+ ions occupy interstitial positions, the LTP structure can be represented by,[12]

$$1\ Li^+ \cdot 2\ [TiO_{6/2}]^{2-} \cdot 3.0\ [PO_{4/2}]^+$$

For LATP of nominal composition $Li_{1.3}Al_{0.3}Ti_{1.7}[PO_4]_3$, an NMR-derived Al_T/Al_O ratio of *ca.* 0.25 implies that at most 80% of the total Al added is incorporated into the LTP structure. If $AlPO_4$ were the only impurity phase present, then the modified ceramic composition could be approximated by

$$1.3\ Li^+ \cdot 0.24\ [AlO_3]^{3-} \cdot 1.7\ [TiO_3]^{2-} \cdot 2.94\ [PO_2]^+$$

where vacancies are present and the material can be considered as Li rich. In reality, small quantities of rutile and TiP_2O_7 are also present, rendering the true stoichiometry of the modified ceramic difficult to establish.

A hypothesis. Based on the ^{27}Al MAS and XRD results presented in this study, the enhanced ionic conductivity found for the modified LTP ceramics can be correlated to increasing Al added, both in terms of direct substitution and the presence of tridymite. Structural and compositional changes resulting from framework modification lead to two implications, vacancies and grain boundary phases, both of which may influence lithium ion dynamics in the modified LTP framework. Vacancies are well known to promote diffusion in a crystal and thereby affect bulk ionic conductivity. Impurity phases present at the inter-crystalline regions are important space fillers to reduce porosity in a pellet. More importantly, these grain boundary phases (in this work postulated to be tridymite) may provide low energetic pathways for charge transport through the intergranular regions. This interpretation is consistent with the observed reduction in the activation energy for grain boundary conductivity observed by Aono *et al.* in LATP.[3,4]

Conclusion

Two ^{27}Al MAS signals have been observed in the families of modified LTP ceramics, and they have been assigned to Al in octahedral (δ −15) and tetrahedral (δ 40) sites. The octahedral signal was assigned to aluminium in the octahedral sites of the LTP framework, and thus confirmed the incorporation of Al into LTP. The signal at δ 40 was assigned to Al in the tridymite phase of $AlPO_4$, the presence of which was also detected by X-ray powder diffraction. ^{27}Al NMR showed increasing aluminium incorporation into LTP as well as increasing presence of $AlPO_4$ (tridymite) with increasing Al added. Tridymite was much more prominently present in LATP and V-LATP than in Nb-LATP. The ^{31}P MAS lineshape changes were interpreted as increasing LTP structural distortion resulting from Al occupying the Ti sites. The effects of V or Nb substitutions were confirmed by the observation of minor resonances separated from the main resonance. The presence of $AlPO_4$, and other impurity phases, suggests that the modified LTP ceramics are non-stoichiometric and contain vacancies. In combination with changes in the unit cell parameters derived from analyses of X-ray powder diffraction patterns, we propose that the enhanced bulk lithium ion conductivity (observed by Aono *et al.* and repeated in our laboratory) can be correlated to both the incorporation of aluminium and the presence of vacancies in the LTP framework, while the improved grain boundary conductivity can be correlated to the presence of grain boundary phase(s) possibly the tridymite phase of $AlPO_4$.

References

1 J. B. Goodenough, H. Y.-P. Hong and J. A. Kafalas, *Mater. Res. Bull.*, 1976, **11**, 203.
2 M. A. Subramanian, R. Subramanian and A. Clearfield, *Solid State Ionics*, 1986, **18/19**, 562.
3 H. Aono, E. Sugimoto, Y. Sadaoka, N. Imanaka and G.-y. Adachi, *J. Electrochem. Soc.*, 1989, **136**, 590.
4 H. Aono, E. Sugimoto, Y. Sadaoka, N. Imanaka and G.-y. Adachi, *Chem. Lett.*, 1990, **1990**, 1825.
5 A. B. Best, K. M. Nairn, S. Wong, P. J. Newman, D. R. MacFarlane and M. Forsyth, *Proceedings of the 18th Australasia Ceramics Conference*, *Sept.*, *1998*, *Melbourne, Australia*.
6 K. M. Nairn, M. Forsyth, M. Greville, D. R. MacFarlane and M. E. Smith, *Solid State Ionics*, 1996, **86–88**, 1397.
7 *Nat. Bur. Stand. U.S. Monogr.*, 1984, **25** (21), 79.
8 *Nat. Bur. Stand. U.S. Circ.*, 1960, **539**, 10, 4.
9 D. Tran Qui and E. Prince, *Z. Kristallogr.*, 1988, **183**, 293.
10 D. Tran Qui, S. Hamdoune, J. L. Soubeyroux and E. Prince, *J. Solid State Chem.*, 1988, **72**, 309.
11 D. Tran Qui and S. Hamdoune, *Acta Crystallogr.*, *Sect. C*, 1988, **44**, 1360.
12 K. C. Sobha and K. J. Rao, *J. Solid State Chem.*, 1996, **121**, 197.
13 Y. Nan, W. E. Lee and P. F. James, *J. Am. Ceram. Soc.*, 1992, **75**, 1641.
14 V. O. W. Flörke, *Z. Kristallogr.*, 1967, **125**, 134.
15 D. Müller, E. Jahn and G. Ladwig, *Chem. Phys. Lett.*, 1984, **109**, 332.
16 R. D. Shannon, *Acta Crystallogr.*, *Sect. A*, 1976, **32**, 751.
17 L. Pauling *The Nature of the Chemical Bond*, Cornell University Press, Ithaca, NY, 3rd edn., 1960.

Paper 8/02752H